Decentralised approaches to Anti-windup Design with Application to Quadrotor Unmanned Aerial Vehicles

Nkemdilim A. Ofodile[a,b] and Matthew C. Turner[a]

***Abstract*—This paper considers the design of structured anti-windup compensators for open-loop stable plants which themselves have a particular structure: a diagonal dynamic part cascaded with a static, invertible part. Two approaches to the design of such compensators are proposed. The first is a pseudo-decentralised anti-windup compensator which is a direct extension of a similar scheme in the literature. The second approach allows anti-windup compensators to be designed individually for each control channel and, provided a certain linear program is satisfied, allows the compensators to be implemented in such a way that the nonlinear closed-loop is asymptotically stable. The design approaches are applied to a quadrotor UAV, which inspired the work, and results from both simulations and flight tests are reported.**

I. Introduction

For control systems experiencing actuator saturation, anti-windup (AW) compensators are designed to work with existing controllers to prevent excessive degradation in performance during periods of saturation and to quickly allow the system to return to normal operation after saturation has occurred. The topics of actuator saturation and AW compensation techniques have been studied extensively over the past two decades and a number of useful anti-windup techniques are now available [1], [2], [3], [4]. In recent years several books have also been written on the subject [5], [6], [7] and a tutorial is also available [8].

Despite the advances made over recent years, the performance of most anti-windup compensators in much of the literature is normally demonstrated using single-input-single-output (SISO) systems. Although most of the design approaches can, in principle, be applied to multi-input-multi-output (MIMO) systems, these tests are often not performed and in certain cases performance can be disappointing. At least part of this may be due to the difficulty of interpreting the practical consequences of $\mathcal{L}_2$ performance for multivariable systems. Two papers which have recently examined this are [9] and [10]. A further disadvantage of MIMO anti-windup compensators is their lack of structure which may deprive the compensators of transparency and may allow their theoretical advantages to be overshadowed by structural drawbacks when applied in practice.

In this paper, we re-visit the problem of anti-windup design for MIMO systems and provide structure to the anti-windup compensators in order to simplify their implementation and enhance the transparency of their operation. In particular, we provide two approaches for the design of structured compensators for plants which consist of a diagonal dynamic part, preceded by an invertible, static part. Practical systems that fall into this class of MIMO systems include, but are not restricted to, quadrotor unmanned air vehicles (UAVs). The AW design techniques considered here follow the approach for full order multivariable AW compensator design proposed in [4] but extend these results in two different directions. The first extension exploits the structure of the plant in order to impose a certain AW compensator structure: this results in an AW compensator which, in a certain sense, is decentralised - we say it is *pseudo-decentralised*. The second extension shows how a MIMO AW compensator can be constructed from a combination of single-loop anti-windup compensators which can be designed in isolation. These compensators are referred to as channel-by-channel AW compensators [11], [12], and have the advantage that they can be designed purely using a set of SISO systems, which greatly simplifies their tuning.

Any anti-windup compensator must ensure that their use guarantees stability of the overall system and hence the paper presents stability analyses which provide conditions which the anti-windup compensators must satisfy. These stability conditions follow on naturally from the method in [4] for the pseudo-decentralised approach and, as with most other advanced anti-windup techniques, can be cast as a set of linear matrix inequalities. The channel-by-channel approach is accompanied by more stringent stability criteria which consist of a set of linear matrix inequalities for each channel of the *design*, and, in addition a linear program which must be feasible for stability to be ensured. In both approaches, there is a trade-off between architectural simplicity and feasibility of the stability conditions, compared to the approach of [4]. However, in practical situations, architectural simplicity and transparency are often highly valued.

The inspiration for this work was the development of anti-windup compensators in order to alleviate saturation problems in quadrotor UAVs where, for reasons of ease of implementation and monitoring, a set of single-loop anti-windup compensators are preferred to one multivariable compensator. A number of researchers have reported the problem of actuator saturation in quadrotors to exist in normal flight situations and extreme maneuvers [13], [14], [15]. The proposed anti-windup compensators are designed and integrated into a modified 2014 3DR Quadrotor UAV and compared to the MIMO anti-windup method of [4] in both simulation and flight-test. Results of flight tests from this integration are presented to show the improved performance of the quadrotor UAV during saturation of its motors.

[a] Nkemdilim Ofodile and Matthew Turner are with the Department of Engineering, University of Leicester, Leicester, UK. {nao9,mct6}@leicester.ac.uk

[b] Nkemdilim Ofodile works at Air Force Institute of Technology, Kaduna, Nigeria nkedilim.ofodile@airforce.mil.ng

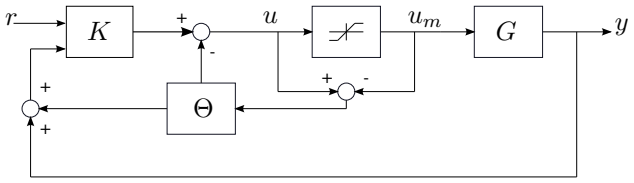

Fig. 1. Single-loop anti-windup structure

Notation: Notation in this paper is standard. $\mathcal{R}^{m\times p}$ denotes the space of real rational $m \times p$ transfer function matrices; the subspace which is analytic in the closed right half plane is denoted $\mathcal{RH}_\infty^{m\times p}$. If dimensions are unimportant, $\mathcal{RH}_\infty$ is often used as short-hand.

A signal $x(t) \in \mathcal{L}_2$ if its $\mathcal{L}_2$ norm

$$\|x\|_2 := \left(\int_0^\infty \|x(t)\|^2 dt\right)^{\frac{1}{2}}$$

is finite. The $\mathcal{L}_2$ gain or induced $\mathcal{L}_2$ norm of a (nonlinear) mapping $\mathcal{T}(.)$ is defined as

$$\|\mathcal{T}\|_{i,2} := \sup_{0\neq x\in\mathcal{L}_2} \frac{\|\mathcal{T}(x)\|_2}{\|x\|_2}.$$

The saturation function is defined as

$$\mathrm{sat}(u) := [\mathrm{sat}(u_1), \ldots, \mathrm{sat}(u_m)]'$$

and $\mathrm{sat}(u_i) := \min\{|u_i|, \bar{u}_i\} \times \mathrm{sign}(u_i)$. The deadzone function given as

$$\mathrm{Dz}(u) := u - \mathrm{sat}(u)$$

and $\mathrm{Dz}(u_i) = \max\{0, |u_i| - \bar{u}_i\} \times \mathrm{sign}(u_i)$. $\tilde{u}$ is used to replace $\mathrm{Dz}(u)$ in some parts of this paper. The notation $\mathrm{He}\{A\}$ is given as

$$\mathrm{He}\{A\} = A + A'.$$

II. Two special cases of anti-windup design

Before presenting the main results of the paper, it is fruitful to consider two special cases of anti-windup design: full-order anti-windup design for MIMO systems and its counterpart for single-loop, or SISO, systems (actually the systems are SIMO because allowance is made for the controller to access more than one output). Consideration of the MIMO case is important for the development of the pseudo-decentralised results considered later; consideration of the SIMO case is important for the development of the channel-by-channel approach which is finally developed.

A. Full-order anti-windup design for MIMO systems

This section reviews the approach to full-order anti-windup design described in [4] (see also [16]). A full-order anti-windup compensator has the same order as the plant, $G(s)$. Its main advantage is that, for stable systems $G(s) \in \mathcal{RH}_\infty$, a globally stabilising full-order compensator always exists. The pseudo-decentralised approach to anti-windup design we present later builds on the approach presented below.

Consider Figure 1 which shows a generic anti-windup configuration. It is assumed that the plant $G(s) \in \mathcal{RH}_\infty^{p\times m}$ and that the controller $K(s)$ stabilises the plant in the absence of saturation. $\Theta(s)$ is the anti-windup compensator which only becomes active once saturation has occurred. In this figure

- $u, u_m \in \mathbb{R}^m$ are the control signal and plant input respectively.
- $r \in \mathbb{R}^{n_r}$ is the reference and $y \in \mathbb{R}^p$ is the plant output.

The plant $G(s)$ has the following state-space realisation

$$G(s) \sim \left[\begin{array}{c|c} A_p & B_p \\ \hline C_p & D_p \end{array}\right] \tag{1}$$

where $A_p \in \mathbb{R}^{n_p\times n_p}$. For simplicity, disturbances are not considered, and they have no impact on the stability analysis. Based on the formulation for full-order AW compensators in [17], [18], the following structure:

$$\Theta(s) = \begin{bmatrix} M(s) - I \\ G(s)M(s) \end{bmatrix} \tag{2}$$

is chosen for $\Theta(s)$ where the transfer function $M(s) \in \mathcal{RH}_\infty^{m\times m}$ is chosen as part of a right coprime factorisation of the plant $G(s) = N(s)M(s)^{-1}$. If this coprime factorisation is chosen to be equal in order to that of the plant, a state-space realisation of the anti-windup compensator can therefore be given by

$$\Theta(s) = \begin{bmatrix} M(s) - I \\ N(s) \end{bmatrix} \sim \left[\begin{array}{c|c} A_p + B_pF & B_p \\ \hline F & 0 \\ \hline C_p + D_pF & D_p \end{array}\right] \tag{3}$$

where F is chosen such that $A_p + B_pF$ is Hurwitz. With this choice of anti-windup compensator, it can be shown ([17]) that Figure 1 is mathematically equivalent to Figure 2. Figure 2 is more useful for analysis of the system with saturation and anti-windup because it is partitioned into three distinct subsystems. Under the assumption that $K(s)$ stabilises $G(s)$ and gives desirable behaviour, it follows that (i) the entire system is stable if and only if the nonlinear loop is stable; and (ii) the performance of the system is governed by the mapping $\mathcal{T}_p : u_{lin} \mapsto y_d$. This mapping represents the deviation of the real output (y) from the nominal output (y_{lin}) when saturation and/or anti-windup is active. This approach transforms the AW design problem to that of finding a transfer function matrix $M(s)$ (or equivalently a state-feedback matrix F), such that the nominal closed-loop system with AW compensation is asymptotically stable and the mapping $\mathcal{T}_p$ is well-defined and such that, for some sufficiently small $\gamma > 0$, $\|\mathcal{T}_p\|_{i,2} < \gamma$. The following is a summary of some results from [4].

Theorem 1: Assume that $G(s) \in \mathcal{RH}_\infty^{p\times m}$ and that the nominal interconnection of $K(s)$ and $G(s)$ is asymptotically stable and well-posed. If there exist matrices $Q > 0$, diagonal $U > 0$ and L, and a scalar $\gamma > 0$ such that the following linear matrix inequality

$$\mathrm{He}\left\{\begin{bmatrix} A_pQ + B_pL & B_pU & 0 & 0 \\ -L & -U & I & 0 \\ 0 & 0 & -\frac{\gamma}{2}I & 0 \\ C_pQ + D_pL & D_pU & 0 & -\frac{\gamma}{2}I \end{bmatrix}\right\} < 0 \tag{4}$$

holds, then the anti-windup compensator (3) with $F = LQ^{-1}$ ensures that the system in Figure 2 is globally exponentially stable, well posed and such that $\|\mathcal{T}_p\|_{i,2} < \gamma$.

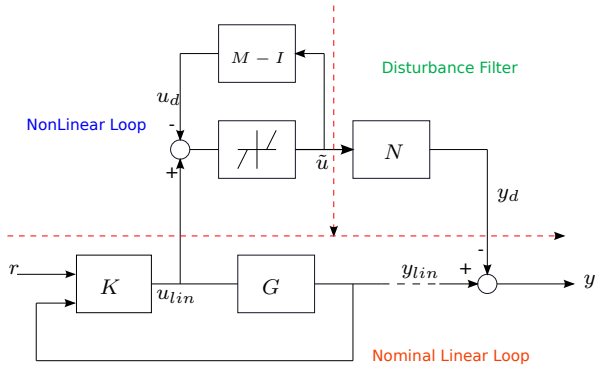

Fig. 2. Equivalent representation of structure

The above theorem does not require the plant and the controller to have a specific structure and, indeed, can be applied to any stable plant $G(s)$ with a stabilising linear controller, $K(s)$. However, one might expect that if the plant and controller have structure, some simplifications of this result could be obtained.

B. Full-order anti-windup design for SIMO systems

A useful special case of the generic MIMO result can be obtained when the system in question has only one control input (but possibly more than one output measurement). Consider Figure 3 where $G_i(s) \in \mathcal{RH}_\infty^{p_i \times 1}$ is the plant, $K_i(s)$ is the controller and $\Theta_i(s)$ is the anti-windup compensator. A state-space realisation for the plant, $G_i(s)$, is

$$G_i(s) \sim \left[\begin{array}{c|c} A_i & B_i \\ \hline C_i & D_i \end{array}\right] \tag{5}$$

where $A_i \in \mathbb{R}^{n_i \times n_i}$. Similarly to Section II-A, $u, u_m \in \mathbb{R}$ are the control signal and plant input respectively, $r \in \mathbb{R}$ is the reference, $y \in \mathbb{R}^{p_i}$ is the plant output. All other signals have compatible dimensions. The anti-windup compensator $\Theta_i(s)$ has the same structure as in equation (3), where

$$\Theta_i(s) = \begin{bmatrix} M_i(s) - 1 \\ N_i(s) \end{bmatrix} \sim \left[\begin{array}{c|c} A_i + B_i F_i & B_i \\ \hline F_i & 0 \\ \hline C_i + D_i F_i & D_i \end{array}\right]. \tag{6}$$

As with Section II-A, this structure of anti-windup compensator allows Figure 3 to be re-drawn as the mathematically equivalent diagram, Figure 4. Again, the mapping $\mathcal{T}_p : u_{lin} \mapsto y_d$ governs the deviation of performance from nominal due to saturation and influence of the anti-windup compensator. The following is then a special case of Theorem 1.

Theorem 2: Assume that $G_i \in \mathcal{RH}_\infty^{p_i \times 1}$ and that the nominal interconnection of $K_i(s)$ and $G_i(s)$ is asymptotically stable

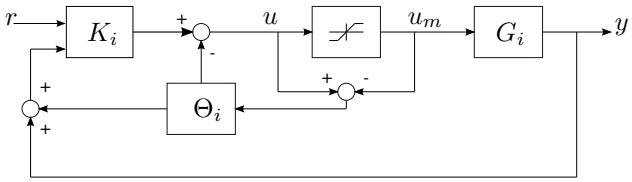

Fig. 3. Single-loop anti-windup structure

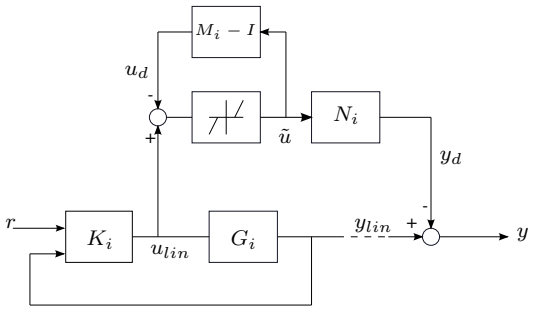

Fig. 4. Equivalent representation of single-loop anti-windup structure

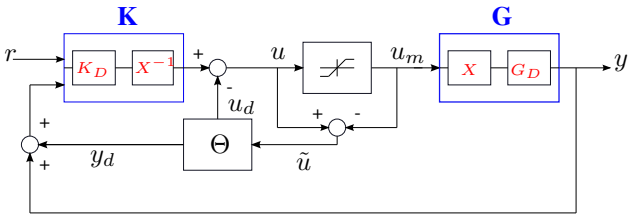

Fig. 5. Full anti-windup structure

and well-posed. If there exist matrices $Q_i > 0$, L_i and scalars $U_i > 0$ and $\gamma_i > 0$ such that the following linear matrix inequality

$$\text{He}\left\{\begin{bmatrix} A_i Q_i + B_i L_i & B_i U_i & 0 & 0 \\ -L_i & -U_i & I & 0 \\ 0 & 0 & -\frac{\gamma_i}{2} & 0 \\ C_i Q_i + D_i L_i & D_i U_i & 0 & -\frac{\gamma_i}{2} I \end{bmatrix}\right\} < 0 \tag{7}$$

holds, then the system in Figure 4, with the anti-windup compensator in equation (6) where $F_i = L_i Q_i^{-1}$, is globally exponentially stable, well posed and such that $\|\mathcal{T}_p\|_{i,2} < \gamma_i$.

If $\mathcal{L}_2$ gain is not important, the following corollary may be used instead.

Corollary 1: Assume that $G_i \in \mathcal{RH}_\infty^{p_i \times 1}$ and that the nominal interconnection of $K_i(s)$ and $G_i(s)$ is stable and well-posed. If there exist matrices $Q_i > 0$, L_i and scalars $U_i > 0$ such that the following linear matrix inequality

$$\begin{bmatrix} Q_i A_i' + A_i Q_i + B_i L_i + L_i' B_i' & B_i U_i - L_i' \\ \star & -2U_i \end{bmatrix} < 0 \tag{8}$$

holds, then the system in Figure 4, with the anti-windup compensator (6) where $F_i = L_i Q_i^{-1}$, is globally exponentially stable, well posed and there exists a $\gamma_i > 0$ such that $\|\mathcal{T}_p\|_{i,2} < \gamma_i$.

The choice of U_i in this case is not important and does not affect feasibility of (8) or the design of the anti-windup compensator. To see this, note that inequality (8) can be divided by U_i to eliminate it from the LMI, resulting in a scaling of L_i and Q_i by the same factor: but as $F_i = L_i Q_i^{-1}$, the net effect of U_i on F_i is zero.

III. Anti-windup Design for a Class of MIMO Systems

Consider now Figure 5. The signals and systems have the same meaning as defined in Section II-A, but it is now assumed

that the plant $G(s)$ and the controller $K(s)$ have the special structures

$$G(s) = G_D(s)X, \qquad K(s) = X^{-1}K_D(s) \tag{9}$$

where $X \in \mathbb{R}^{m\times m}$ is a static nonsingular matrix whose inverse can be considered as a control allocation matrix and,

$$G_D(s) = \text{blockdiag}(G_1(s), G_2(s), \ldots, G_m(s)) \tag{10}$$
$$K_D(s) = \text{blockdiag}(K_1(s), K_2(s), \ldots, K_m(s)) \tag{11}$$

Here it is assumed that each $G_i(s) \in \mathcal{RH}_\infty^{p_i\times 1}$ and that $\sum_{i=1}^m p_i = p$. The controller dimensions are consistent with this. State-space realisations for $G_i(s)$, $i \in \{1,\ldots,m\}$ are the same as those given in equation (5) where $\sum_{i=1}^m n_i = n_p$. Due to the invertibility assumption on X, when no saturation occurs, the system behaves as m decoupled SISO (or more accurately SIMO) systems with each $K_i(s)$ responsible for controlling the corresponding $G_i(s)$. Unfortunately, if saturation occurs, the decoupling into single feedback loops offered in the unsaturated (nominal) case is ruined because of the presence of X. This is because the nonlinear operation represented by $\chi(.) : \mathbb{R}^m \mapsto \mathbb{R}^m$, where

$$\chi(v) := X\text{sat}(X^{-1}v)$$

is not decentralised. Hence during saturation, the system experiences windup and becomes vulnerable to performance degradation due to directionality [9]. It is important to note that if saturation occurs and X is diagonal, the decoupling effect we desire is restored. Therefore, in general, if anti-windup compensators $\Theta_i(s)$ were designed for each i'th feedback loop independently, it would be unreasonable to expect them to work on the fully coupled system due to the static effects of X. Conversely, due to the structure of the controller and plant, one might expect an anti-windup compensator with a simpler structure than the generic MIMO one described in Section II-A to be obtained.

Before proceeding further it is important to state the following standing assumption made throughout the paper.

Assumption 1:

1) The plant and controller have the structures (9)-(11)
2) The unconstrained closed-loop interconnection of the plant $G(s)$ (10) and controller $K(s)$ (11) is well-posed and asymptotically stable
3) $G(s) \in \mathcal{RH}_\infty$ (and by extension each $G_i(s)$ for $i \in \{1,\ldots,m\}$ is stable i.e. $G_i(s) \in \mathcal{RH}_\infty$)

Under Assumption 1, the next subsections will present two different approaches to anti-windup design for this special class of system.

A. Pseudo-decentralised Anti-windup Design

Consider again Figure 5 and assume that the plant and controller are structured as described above. The anti-windup compensator is driven by the signal $\tilde{u} = u - u_m = \text{Dz}(u)$. However, Figure 5 can be re-drawn more conveniently as Figure 6, where

$$\tilde{\Theta} = \begin{bmatrix} X \\ I \end{bmatrix} \Theta X^{-1}. \tag{12}$$

In this case our *virtual* anti-windup compensator, $\tilde{\Theta}(s)$ can be considered to be driven by the signal

$$\tilde{v} = v - v_m = v - \chi(v).$$

It is also convenient to note that

$$\tilde{v} = \tilde{\chi}(v) := X\text{Dz}(X^{-1}v).$$

The control output u and plant input u_m in Figure 5 are real signals and direct consequences of the saturation function. However the signals v and v_m in Figure 6 represent imaginary or virtual signals which are the result of the plant and controller structure $G(s) = G_D(s)X$ and $K(s) = X^{-1}K_D(s)$. For this reason, the anti-windup compensator is described as pseudo-decentralised; it is only decentralised from the perspective of the virtual signals, not the *physical* signals.

Assuming the virtual AW compensator $\tilde{\Theta}(s)$ is

$$\tilde{\Theta}(s) = \begin{bmatrix} \tilde{\Theta}_1(s) \\ \tilde{\Theta}_2(s) \end{bmatrix}$$

and by isolating the nonlinear operator $\chi(v)$ as a single entity with input v and output v_m, it is possible to re-interpret the effect of anti-windup on the closed loop in a similar manner to [17]. From Figure 7, it can be seen that

$$y = G_D v_m = G_D[v - \tilde{v}].$$

Since, $v = v_{lin} + v_d$, and $v_d = \tilde{\Theta}_1\tilde{v}$,

$$y = G_D v_{lin} - G_D[\tilde{\Theta}_1 + I]\tilde{v}. \tag{13}$$

Given that, $y_{lin} = y + y_d$, $y_d = \tilde{\Theta}_2\tilde{v}$ then

$$y_{lin} = G_D v_{lin} - G_D(\tilde{\Theta}_1 + I)\tilde{v} + \tilde{\Theta}_2\tilde{v}. \tag{14}$$

Therefore, the virtual AW compensator is chosen to have the form

$$\tilde{\Theta}(s) = \begin{bmatrix} \tilde{\Theta}_1(s) \\ \tilde{\Theta}_2(s) \end{bmatrix} = \begin{bmatrix} M_D(s) - I \\ G_D(s)M_D(s) \end{bmatrix} \tag{15}$$

where $M_D(s) \in \mathcal{RH}_\infty^{m\times m}$ is some transfer function matrix. As with Section II-A, the equivalent representation in Figure 6 is shown in Figure 7. Note that, because $G_D(s)$ is block-diagonal, it is possible (and desirable) to choose $M_D(s)$ block-diagonal as well. Therefore $\tilde{\Theta}(s)$ is de-centralised, implying a pseudo-decentralised anti-windup design structure from the point of view of the physical signals. Again, note the same decoupled structure. The nonlinear loop in Figure 7 is described by the following equation:

$$\tilde{v} = XDz(X^{-1}v).$$

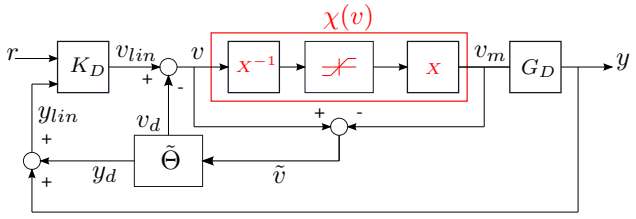

Fig. 6. Decentralised AW structure

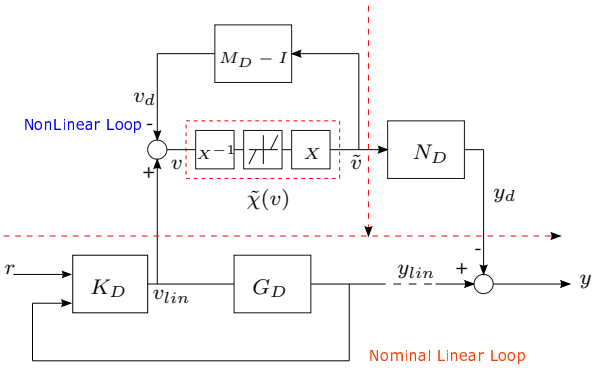

Fig. 7. Equivalent representation of decentralised AW structure

Since $v = v_{lin} - v_d$, then

$$\tilde{v} = XDz[X^{-1}(v_{lin} - v_d)]. \tag{16}$$

The stability and performance of the system with the pseudo-decentralised AW compensation is dependent on ensuring that the nonlinear operator $\mathcal{T}_p : v_{lin} \mapsto y_d$ is stable and that its $\mathcal{L}_2$ gain is sufficiently small. Taking inspiration from the previous sections, and noting that $G_D(s)$ is a block diagonal transfer function matrix with state-space realisation

$$G_D(s) \sim \left[\begin{array}{c|c} A_D & B_D \\ \hline C_D & D_D \end{array}\right] \tag{17}$$

where

$$A_D = \text{blockdiag}\,(A_1, \ldots, A_m) \tag{18}$$
$$B_D = \text{blockdiag}\,(B_1, \ldots, B_m) \tag{19}$$
$$C_D = \text{blockdiag}\,(C_1, \ldots, C_m) \tag{20}$$
$$D_D = \text{blockdiag}\,(D_1, \ldots, D_m), \tag{21}$$

it then follows that a coprime-factor based virtual anti-windup compensator $\tilde{\Theta}(s)$ has the following structure:

$$\tilde{\Theta}(s) = \begin{bmatrix} M_D(s) - 1 \\ N_D(s) \end{bmatrix} \sim \left[\begin{array}{c|c} A_D + B_D F_D & B_D \\ \hline F_D & 0 \\ \hline C_D + D_D F_D & D_D \end{array}\right] \tag{22}$$

where

$$F_D = \text{blockdiag}\,(F_1, \ldots, F_m). \tag{23}$$

Conditions which can be used to provide an anti-windup compensator guaranteeing stability and finite $\mathcal{L}_2$ gain can now be given.

Theorem 3: Let Assumption 1 be satisfied. Then there exists an anti-windup compensator of the structure (12) such that the origin of the system in Figure 7 is globally asymptotically stable and $\|\mathcal{T}_p\|_{i,2} < \gamma$ if there exist block-diagonal matrices $Q_D > 0$ and L_D, a diagonal matrix $U_D > 0$ and a positive real scalar γ such that the following LMI

$$\text{He}\left\{\begin{bmatrix} A_D Q_D + B_D L_D & B_D X U_D & 0 & 0 \\ -L_D X^{-1} & -X^{-1} U_D & X^{-1} & 0 \\ 0 & 0 & -\frac{\gamma}{2} I & 0 \\ C_D Q_D + D_D L_D & D_D U_D & 0 & -\frac{\gamma}{2} I \end{bmatrix}\right\} < 0. \tag{24}$$

is satisfied. Furthermore, if this inequality is satisfied, a suitable $\tilde{\Theta}(s)$ achieving global asymptotic stability and $\|\mathcal{T}_p\|_{i,2} < \gamma$ is obtained via the state-space equations (22) where F_D as $F_D = L_D {Q_D}^{-1}$.

Proof: See Appendix A.

Remark 1: Compared to the coprime factor based multivariable synthesis method of [4], the result above is more stringent: for the existence of the pseudo-decentralised compensator described in equation (22) a more restrictive LMI must be satisfied (24): this is the price paid for a pseudo-decentralised structure. □

B. Channel-by-channel anti-windup synthesis

The structure of Figure 8 is a slightly modified version of Figure 6. Here, the AW compensator receives its input $\tilde{u}$ directly from the saturation function. Since the AW compensator has the transfer function $\Theta(s) = [\Theta_1(s) \quad \Theta_2(s)]'$ and $\tilde{u} = \text{Dz}(u)$, it then follows that

$$\begin{aligned} y &= G_D X u_m \\ &= G_D X[u - \tilde{u}] \\ &= G_D(u_{lin} - \Theta_1 \tilde{u}) - G_D X \tilde{u} \\ &= G_D u_{lin} - G_D[\Theta_1 + X]\tilde{u}. \end{aligned} \tag{25}$$

Similar to the process followed in Section III-A, noting $y_{lin} = y + y_d$ and choosing $\Theta_1(s) = M(s) - X$ yields

$$\begin{aligned} y_{lin} &= G_D u_{lin} - G_D(\Theta_1 + X)\tilde{u} + \Theta_2 \tilde{u} \\ &= G_D u_{lin} - G_D M \tilde{u} + \Theta_2 \tilde{u}. \end{aligned} \tag{26}$$

For $y_{lin} = G_D u_{lin}$, let $\Theta_2(s) = G_D(s)M(s)$. Therefore our AW compensator has the generic form:

$$\Theta(s) = \begin{bmatrix} \Theta_1(s) \\ \Theta_2(s) \end{bmatrix} = \begin{bmatrix} M(s) - X \\ G_D(s)M(s) \end{bmatrix} \tag{27}$$

where $M(s) \in \mathcal{RH}_\infty^{m \times m}$ is a free parameter to be chosen. The equivalent representation of Figure 8 is shown in Figure 9.

Now, assuming that each $G_i(s)$ has right coprime factorisation

$$G_i(s) = N_i(s) M_i(s)^{-1}$$

and if for $\forall i \in \{1 \ldots, m\}$,

$$\begin{aligned} N_D(s) &= \text{blockdiag}\,(N_1(s), \ldots, N_m(s)) \\ M_D(s) &= \text{blockdiag}\,(M_1(s), \ldots, M_m(s)). \end{aligned}$$

The transfer function matrix $G_D(s)$ has a coprime factorization

$$G_D(s) = N_D(s) M_D(s)^{-1} \tag{28}$$

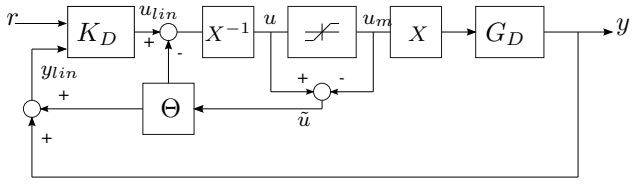

Fig. 8. Applying the AW on general plant structure (MIMO)

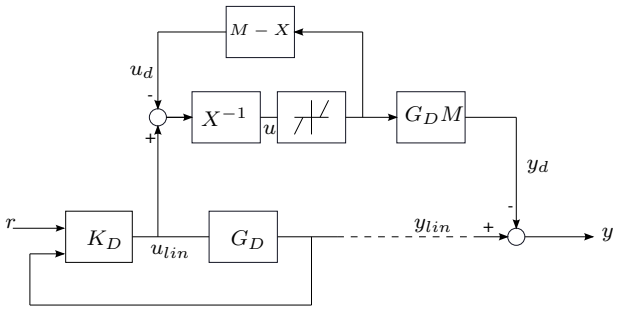

Fig. 9. Equivalent representation for channel-by-channel AW

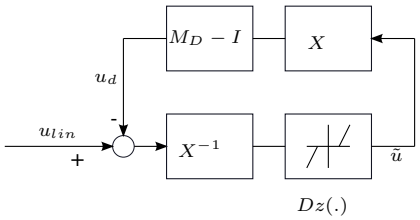

Fig. 10. Non-linear loop for channel-by-channel AW 1

which may be re-written as

$$G_D(s) = N_D(s)X(M_D(s)X)^{-1}. \tag{29}$$

Based on the nonlinear loop in Figure 10, if we choose $M(s) = M_D(s)X$, the linear element becomes

$$M(s) - X = (M_D(s) - I)X.$$

We can then redraw the nonlinear loop of Figure 10 as Figure 11 such that the equations of the *nonlinear loop* then have the form:

$$\tilde{u} = \mathrm{Dz}[X^{-1}(u_{lin} - u_d)] \tag{30}$$

Given that $u_d = (M_D - I)X)\tilde{u}$ then equation (30) becomes

$$\tilde{u} = \mathrm{Dz}[X^{-1}u_{lin} - (X^{-1}(M_D - I)X)\tilde{u}] \tag{31}$$

Hence, the AW compensator now has the form:

$$\Theta(s) = \begin{bmatrix} M_D(s) - I \\ N_D(s) \end{bmatrix} X. \tag{32}$$

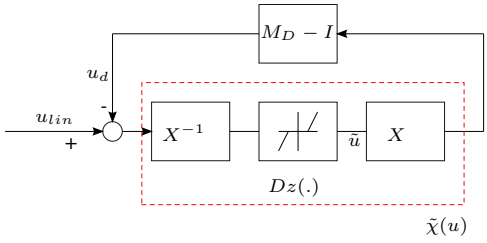

Fig. 11. Non-linear loop for channel-by-channel AW 2

*1) **Stability and performance analysis**:* This section derives conditions which must be satisfied in order for m single-channel anti-windup compensators designed according to Theorem 2 to be combined so that they ensure stability of the overall nonlinear system i.e. they ensure stability of the nonlinear loop in Figure 11. The following lemma is central to the derivation of these results.

Lemma 1: Consider the nonlinearity $\tilde{\chi}(.) : \mathbb{R}^m \mapsto \mathbb{R}^m$

$$\tilde{\chi}(u) := X\mathrm{Dz}(X^{-1}u) \tag{33}$$

where $X \in \mathbb{R}^{m\times m}$ is a nonsingular matrix. If there exist diagonal matrices $W > 0$ and $V > 0$ such that

$$V = X'WX > 0 \tag{34}$$

then the following inequality

$$\tilde{\chi}(u)'W\left(u - \tilde{\chi}(u)\right) \geq 0, \qquad \forall u \in \mathbb{R}^m. \tag{35}$$

holds.

Proof: See Appendix B.

This result can be used to prove, in a similar way to Section III-A, the stability of the system in Figure 9, and therefore Figure 8, as expounded in the following theorem.

Theorem 4: Let Assumption 1 be satisfied. If there exist diagonal matrices $W > 0$ and $V > 0$ such that $V = X'WX$ and there exist matrices $Q_i > 0$, L_i and scalar $U_i > 0$ such that the LMI (8) are satisfied for all $i \in \{1, \ldots, m\}$, then with $\Theta(s)$ designed as in (32) where $F_i = L_iQ_i^{-1}$, the system in Figure 11 is globally exponentially stable.

Proof: See Appendix C.

C. Linear programming solution to sector analysis

The key to the successful implementation of the channel-by-channel anti-windup designs on the multivariable system is Lemma 1: if there exist diagonal matrices $W > 0$ and $V > 0$ such that $V = X'WX$ for the system structure in (9), m AW compensators can designed using the system of LMI's in (8) can be implemented on the multivariable system and stability is assured. The conditions under which there exist matrices $V > 0$ and $W > 0$ such that $V = X'WX$ can be simplified using the $\mathrm{vec}(.)$ operator, where:

$$\mathrm{vec}(X'WX) = \mathrm{vec}(V) = [X' \otimes X']\mathrm{vec}(W) \tag{36}$$

$$= \begin{bmatrix} V_1 \\ 0 \\ \vdots \\ V_2 \\ 0 \\ \vdots \\ \vdots \\ V_m \end{bmatrix} = [X' \otimes X'] \begin{bmatrix} W_1 \\ 0 \\ \vdots \\ W_2 \\ 0 \\ \vdots \\ \vdots \\ W_m \end{bmatrix} \tag{37}$$

where $\mathrm{vec}(V), \mathrm{vec}(W) \in \mathbb{R}^{m^2}$ and $X' \otimes X' \in \mathbb{R}^{m^2\times m^2}$. The operation $\mathrm{vec}(A)$ where $A = [a_1, a_2 \ldots .a_n] \in \mathbb{R}^{n\times n}$ rearranges the column vectors of A in the following way:

$$vec(A) = [a_1' \quad a_2' \quad \cdots \quad a_n']'$$

Equation (36) uses the relationship between the vec operator and the Kronecker product [19]. Equation (37) represents a linear programming feasibility problem which, after some manipulations, can be investigated using any linear program solver. It is important to note that if solutions exist to the linear program mentioned above, then AW compensators that ensure the nonlinear stability of the entire system in Figure 8 can be designed individually for the m control loops or channels of the multivariable system.

Remark 2: The linear programming solution presents a transparent and efficient method of determining the diagonal matrices $V > 0$ and $W > 0$ satisfying equation (34). However the numerical value of V and W are not used in the actual design of the AW compensator: their existence is purely required in order for us to make statements about the nonlinear stability of the overall system. □□

Remark 3: The channel-by-channel approach may, at first sight, seem a restrictive result: the requirement for the existence of positive definite diagonal matrices, V and W satisfying $V = X'WX$ is strong. However, it enables more practical flexibility than the pseudo-decentralised approach: because only the *existence* of V and W is required, this implies that *any* suitable SIMO anti-windup compensator can be used and this may be re-designed without any effect on the stability of the overall system. This of course has great practical appeal. □□□

IV. The Quadrotor Modelling & Simulation Results

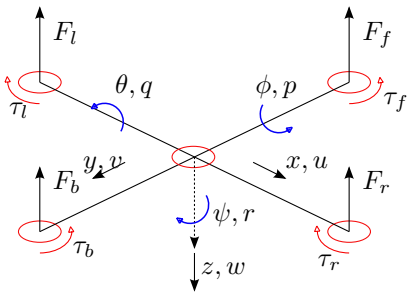

Fig. 12. Force, torque and states definition of a quadrotor

A. *Model Construction*

The quadrotor UAV is an interesting vehicle with great potential for use in many fields and has been studied by many researchers [20], [13], [21].A few researchers have considered the problem of saturation on UAVs, mainly on fixed wing UAVs [22], [23], [24] and fewer than that have studied saturation in UAVs in detail [25].

The structure of a quadrotor is shown in Figure 12. The quadrotor motors each generate an input force and a torque when powered. The quadrotor is controlled by varying the motor speeds, thereby changing the lift force (which is the sum of all input forces) and its six output coordinates (x, y, z position output and ϕ, θ, ψ orientation in space). The pitch of the quadrotor is controlled by one pair of motors (front and back motors) rotating in one direction while the roll is controlled by the other pair of motors (left and right motors) rotating in opposite direction. The yaw movement is obtained by increasing/decreasing the speed of one group of motors while decreasing/increasing the same speed of another group of motors.

The roll, pitch, yaw angles (ϕ,θ, ψ) and the position vector z are the controlled outputs for this quadrotor system where the nonlinear model dynamics (according to [26]) governing the operation of the system is given, with $c = cos(.)$ and $s = sin(.)$, by

$$\begin{bmatrix}\dot{x}\\ \dot{y}\\ \dot{z}\end{bmatrix} = \begin{bmatrix}c\theta c\psi & c\psi s\theta s\phi - c\phi s\psi & c\psi s\theta\cos\phi - s\phi s\psi\\ c\theta s\psi & s\psi s\theta s\phi - c\phi c\psi & s\psi s\theta c\phi - s\phi c\psi\\ -s\theta & c\theta s\phi & c\phi c\phi\end{bmatrix}\begin{bmatrix}u\\ v\\ w\end{bmatrix} \tag{38}$$

$$\begin{bmatrix}\dot{\phi}\\ \dot{\theta}\\ \dot{\psi}\end{bmatrix} = \begin{bmatrix}1 & \sin\phi\tan\theta & \cos\phi\tan\theta\\ 0 & \cos\phi & -\sin\phi\\ 0 & \sin\phi\sec\theta & \cos\phi\sec\theta\end{bmatrix}\begin{bmatrix}p\\ q\\ r\end{bmatrix} \tag{39}$$

$$\begin{bmatrix}\dot{u}\\ \dot{v}\\ \dot{w}\end{bmatrix} = \begin{bmatrix}rv - qw\\ pw - ru\\ qu - pv\end{bmatrix} + \begin{bmatrix}g\sin\theta\\ g\sin\phi\cos\theta\\ g\cos\phi\cos\theta\end{bmatrix} - \frac{1}{m}\begin{bmatrix}0\\ 0\\ F\end{bmatrix} \tag{40}$$

$$\begin{bmatrix}\dot{p}\\ \dot{q}\\ \dot{r}\end{bmatrix} = \begin{bmatrix}\frac{J_y - J_z}{J_x}qr\\ \frac{J_x - J_z}{J_y}pr\\ \frac{J_x - J_y}{J_z}pq\end{bmatrix} + \begin{bmatrix}\frac{1}{J_x}\tau_\phi\\ \frac{1}{J_y}\tau_\theta\\ \frac{1}{J_z}\tau_\psi\end{bmatrix} \tag{41}$$

These dynamics are complex and hence, following [26], by assuming that the roll and pitch angles ϕ, θ and the terms qr, pr and pq in equation (41) (also known as *Coriolis* terms) are small, we can simplify the rotational dynamics to

$$G_D(s) \sim \begin{cases}\ddot{\phi} &= \frac{1}{J_x}\tau_\phi\\ \ddot{\theta} &= \frac{1}{J_y}\tau_\theta\\ \ddot{\psi} &= \frac{1}{J_z}\tau_\psi\\ \ddot{z} &\approx g - \frac{1}{m}F\end{cases} \tag{42}$$

where $\tau_\phi, \tau_\theta, \tau_\psi$ are the roll pitch and yaw torques, F is the total lift force and m, g are the mass of the quadrotor and acceleration due to gravity respectively. Equation (42) shows a simplified structure where the pitch, roll, yaw and height channels are all decoupled; hence we can design the controller easily based on this. Torques (τ^*) and forces (F^*) are generated by each motor and as stated in [26], they can be modelled as

$$F^* = k_1\delta^* \tag{43}$$

$$\tau^* = k_2\delta^* \tag{44}$$

where k_1 and k_2 are constants that are determined experimentally and δ_* is the motor angular velocity squared.

The equations for the total lift force and torques in the roll, pitch and yaw axis as seen in Figure 12 are;

Lift force	$F = F_f + F_r + F_b + F_l$
Roll torque	$\tau_\phi = \alpha(F_l - F_r)$
Pitch torque	$\tau_\theta = \alpha(F_f - F_b)$
Yaw torque	$\tau_\psi = \tau_r + \tau_l - \tau_f - \tau_b$

where α is the distance between the centre of mass of the quadrotor and the motors.

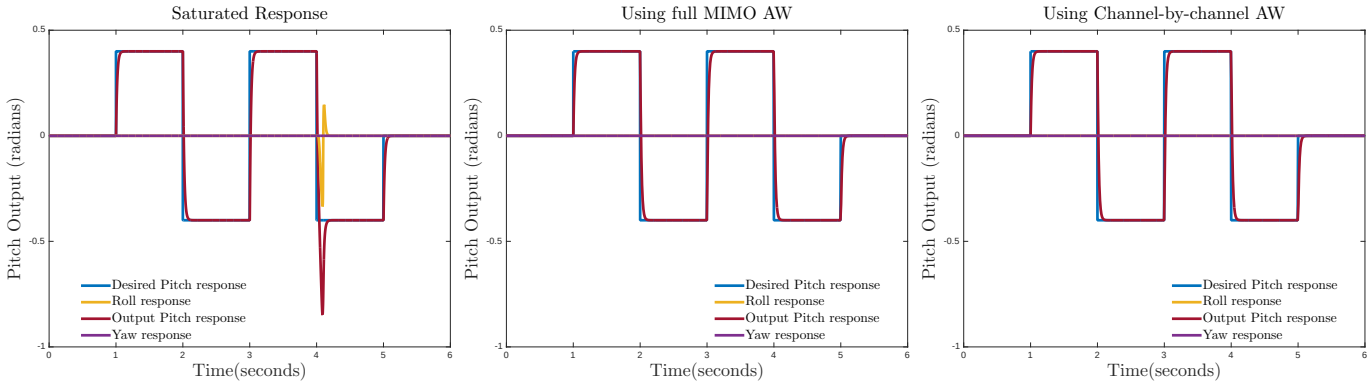

Fig. 13. Pitch angle response: (a) [from left] Saturation, no AW; (b) Saturation, full MIMO AW; and (c) Saturation, channel-by-channel AW

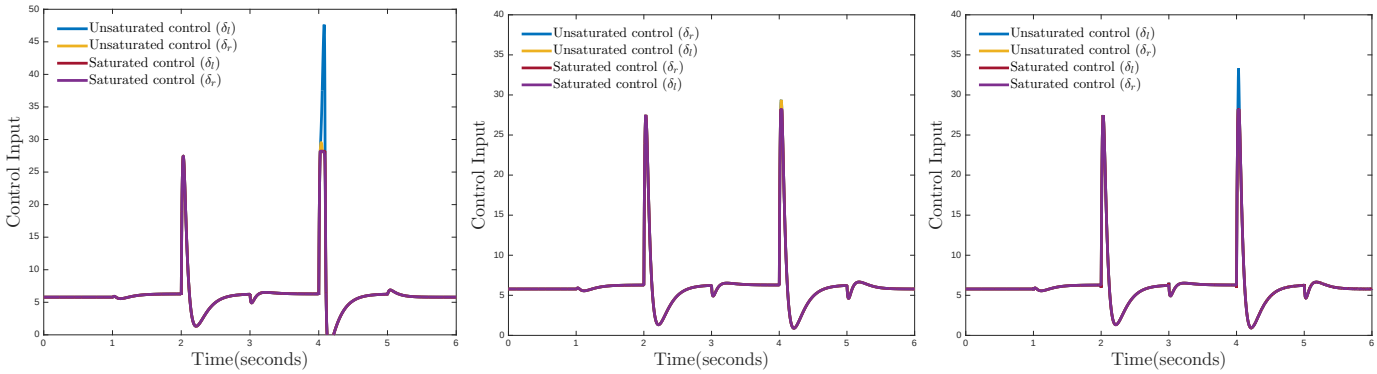

Fig. 14. Control command due to pitch response: (a) [from left] Saturation, no AW; (b) Saturation, full MIMO AW; (c) Saturation, channel-by-channel AW

By substituting the above set of equations into an expanded form of equations (43) and (44), we can then rewrite the forces and torques with respect to the square of the motor angular velocity (which are the actual motor commands) in matrix form as:

$$\begin{bmatrix} F \\ \tau_\phi \\ \tau_\theta \\ \tau_\psi \end{bmatrix} = \underbrace{\begin{bmatrix} k_1 & k_1 & k_1 & k_1 \\ 0 & -\alpha k_1 & 0 & \alpha k_1 \\ \alpha k_1 & 0 & \alpha k_1 & 0 \\ -k_2 & k_2 & -k_2 & k_2 \end{bmatrix}}_{X} \underbrace{\begin{bmatrix} \delta_f \\ \delta_r \\ \delta_b \\ \delta_l \end{bmatrix}}_{u}. \quad (45)$$

Hence equation (45) in conjunction with equation (42) display the structure $G(s) = G_D(s)X$ described in Assumption 1. This structure allows us to design the controller using the form $K(s) = K_D(s)X$ where a simple PD controller is designed for each controlled output that thus makes up $K_D(s)$. The PD controller will not only provide a simple and structured design approach but will also provide stability and control for the angles $\phi, \theta,$ and ψ and position z with satisfactory performance results.

The decoupled structure in equation (42) allow us to design the following decoupled controller for the three angular positions:

$$U_\phi = K_{\phi,P}[r_\phi - \phi] - K_{\phi,D}[p] \quad (46)$$
$$U_\theta = K_{\theta,P}[r_\theta - \theta] - K_{\theta,D}[q] \quad (47)$$
$$U_\psi = K_{\psi,P}[r_\psi - \psi] - K_{\psi,D}[r]. \quad (48)$$

To remain at constant height, the control output must be able to drive its signal to counteract the effects of gravity and hence the PD controller is added to stabilise the motion in z direction. The control law can be described as:

$$U_z = K_{z,P}[r_z - z] - K_{z,D}[w] + g. \quad (49)$$

In equations (48) - (49), the notation definitions are given as

- $K_{\phi,P}, K_{\theta,P}, K_{\psi,P}, K_{z,P}$ are the proportional gains,
- $K_{\phi,D}, K_{\theta,D}, K_{\psi,D}, K_{z,D}$ are the derivative gains,
- $U_{\phi,\theta,\psi,z}$ are the control inputs (in virtual coordinates),
- $r_{\phi,\theta,\psi,z}$are the desired references and
- g is acceleration due to gravity.

B. *Simulation Results*

A fully MIMO AW compensator [4], a pseudo decentralised AW anti-windup compensator (Section III-A) and a set of channel-by-channel anti-windup compensators (Section III-B) were designed using the linear model of the quadrotor system (42). These were then evaluated using the full nonlinear model of the quadrotor. The parameters and PD gains used for the simulation are stated in Table I. These parameters are the same for the physical UAV. Many simulations were used to the evaluate the performance of the anti-windup compensators on the nonlinear model but, for conciseness, only the pitch responses are discussed.

Figure 13 shows the responses of the system when a pulse reference signal of 0.4 radians was commanded on the pitch. The corresponding control response is shown in Figure 14.

TABLE I
APPROXIMATE VALUES OF 3DR QUADROTOR PARAMETERS AND ONLINE PD GAINS

Parameters	Description	Values	Units
g	Gravity	9.81	ms^{-2}
m	Mass	2.1	kg
d	Distance	0.3	m
k_1	Force constant	0.89	
k_2	Torque constant	0.11	
J_x	Pitch Inertia	2.85 x 10^{-6}	kgm^{-2}
J_y	Roll Inertia	2.85 x 10^{-6}	kgm^{-2}
J_z	Yaw Inertia	1.81 x 10^{-6}	kgm^{-2}
$K_{\phi,P}$	Proportional gain	0.22	
$K_{\theta,P}$		0.22	
$K_{\psi,P}$		0.4	
$K_{\phi,D}$	Derivative gain	0.004	
$K_{\theta,D}$		0.004	
$K_{\psi,D}$		0.003	
Throttle via $K_{z,P}$	*Throttle rate* P gain	6	
Throttle via $K_{z,D}$	*Throttle rate* D gain	0.001	

Fig. 15. Modified 2014 3DR Quadrotor

Figures 13a/14a show the saturated response of the system experiencing windup effects of large overshoot on the pitch and roll channels caused by the increasing pitch feedback error driven by slow poles in the nonlinear system and the coupling that exists between the roll and pitch channels.

Figures 13b/14b and 13c/14c clearly show improved responses from the full MIMO AW compensator and the channel-by-channel AW compensator respectively. This implies that rather than have a complex system like the full MIMO AW compensator, a simple channel AW compensator can be designed with ease and this will produce a similar result. A similar output response to the full MIMO AW compensator was obtained for the decentralised AW compensator.

V. FLIGHT TESTING

A. *Test Platform*

The test platform is a 2014 3DR quadrotor [27], a DIY quadrotor kit equipped with the Ardupilot Mega (APM 2.6) programmable flight controller board whose firmware has been modified to allow for the testing and validation of the different AW compensators (See Figure 15). The rotational and translational dynamics of this system is similar to the complete nonlinear dynamics of the quadrotor in Section IV

Flight Controller: The Ardupilot Mega (APM 2.6) is based on the Arduino ATmega2560 microcontroller. It provides a large number of I/O pins for its sensors which include magnetometers, barometric pressure sensors and the inertial measurement unit (IMU) sensor consisting of a three-axis accelerometer and a three-axis gyroscope. The firmware for this system is open source and has a lot of support on cross platform application and programming making it relatively simple to understand and modify.

Components: This quadrotor consists of the following components: (1) four UT2212 850 kV brushless DC motors, (2) a Quattro 4in1 20 A electronic speed controller (ESC) , (3) four 12 inch two-bladed propellers, (4) a Ublox LEA-6H GPS with compass kit (5) a pair of 3DR 433 MHz transceiver telemetry kit (6) an AR6200 6-channel DSMX receiver (7) and a Floureon rechargeable lithium-polymer, 11.1 V, 5500 mAh battery with a power module that supplies variable voltages to the different sections of the quadrotor. See Figure 16 for a block architecture of the interconnections of all these components.

Frame: The 3DR quadrotor frame is a combination of carbon fibre plates and aluminium struts intended to provide a balance between impact strength and weight. Impact strength is required because the frame may take a few hard landings and potential crashes during tests. The central carbon fibre plate is large enough to place components and it makes it easier to attach and detach any components easily for troubleshooting purposes.

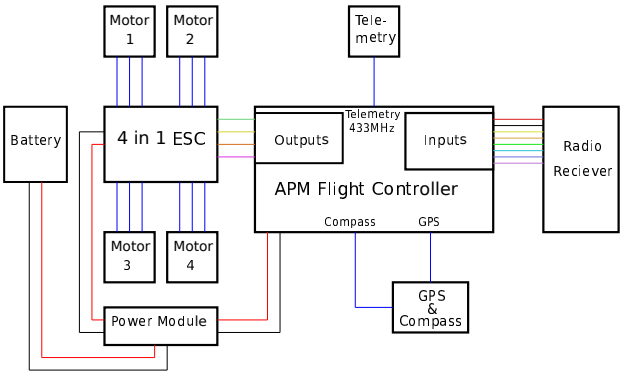

Fig. 16. Quadrotor hardware schematic

Ground Control Station (GCS): The GCS is a computer that runs the software that communicates with the quadrotor remotely via the telemetry system. It helps monitor the quadrotor's performance and status. The GCS software has a heads-up display (HUD), moving maps showing the UAV's position and a host of indicators that help enhance flight performance.

B. *Test Procedure*

For this work, the quadrotor was made to achieve autonomous flight with a constant mission in order to attain a certain level of uniformity in the results gathering. The first stage requires scripting the AW compensators in C code and running it in conjunction with the model in MATLAB/SIMULINK to verify that it functions well. The next stage involves converting the C code to C++ code and adding the scripted

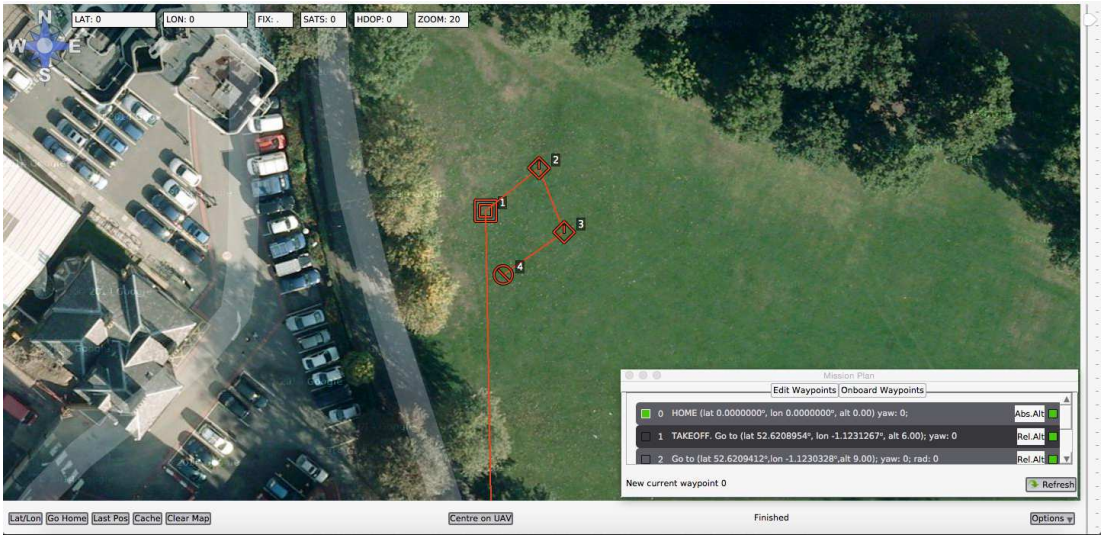

Fig. 17. Snapshot showing Mission Waypoints

C++ code to the already existent PID controller library in the ardupilot firmware code and making a few modifications. A PD controller is derived from the firmware's PID controller by simply setting the integral gain to zero. The final stage involves testing the entire system in a real flight situation. The test in this stage is conducted in the following sequence: (1) first, the UAV is started in manual mode with preflight checks carried out; (2) next, the UAV is switched to autonomous mode while on the ground for the saved mission to begin; (3) as the UAV automatically takes off, it follows the pre defined paths and reference commands set in the mission while it is being monitored from the GCS; (4) finally, after all commands are executed, the UAV lands automatically and shuts down the motors signifying the end of the mission.

The motor commands to be saturated are the angular velocities. However since angular velocities cannot be directly measured by our system, the motor's PWM input value is used instead where the angular velocity is obtained by conversion from RPM values and these RPM values are recorded by the firmware code for various PWM command levels operating with duty cycle range between 1000 μs (1 ms) and 2000 μs (2 ms) at a frequency of 490 Hz. Figure 18 shows the typical PWM conversion ranges for this system where the PWM signal period is 2 ms.

Under gusty conditions, the quadrotor proved vulnerable to the effects of actuator saturation. However, these conditions made tests not repeatable and made it difficult to fly the UAV safely. Therefore, to safely and consistently observe the effects of saturation, artificial limits were imposed on the system using the software and flights only took place in clement weather. This ensured that saturation effects could be recovered from safely (i.e. the limits could be restored to nominal values) to prevent the quadrotor from crashing, and also that saturation arose mainly from (repeatable) reference demands rather than (unrepeatable) disturbances.

In initial tests, the artificial saturation limits were set at about 50% of nominal. However, without AW, the quadrotor became highly unstable and resulted in a safe crash seconds after the artificial limits were engaged. When AW was applied with these limits engaged, the quadrotor maintained stable flight in air but with less than desirable performance. For this reason, artificial limits were degraded to a more modest 13% of nominal in all flight tests, which corresponded to 7350 rpm or 120 rad/s. These modest degradations still allow the differences between the UAV behaviour with and without anti-windup to be observed but the flights were less prone to disaster. In the test performed, the AW is engaged in the

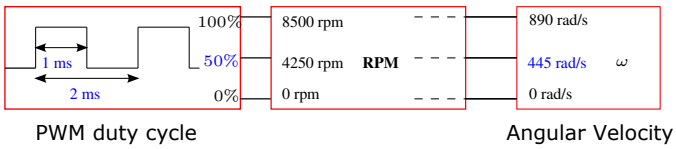

Fig. 18. PWM conversion

mission on the path from waypoint 2 to waypoint 3 at an altitude of 9 m when the quadrotor is on level flight as shown in Figure 17 and then the artificial limits are switched off just before it hits waypoint 3.

C. *Flight Test Results*

Figure 19a shows a typical pitch response during a complete flight for a saturated system with no AW case while Figure 19b shows another complete flight for a saturated system with the channel-by-channel AW case.

Figure 20a focuses on the flight section with the waypoints where artificial limit were applied and shows the response of the system when no artificial saturation limits are imposed on the system. Note the nominal system's good performance with some good signal tracking and good settling time.

Now, Figure 20b shows a degraded response with the artificial saturation limits imposed. It can clearly be seen that the pitch response has large overshoots and is out of phase. Physically,

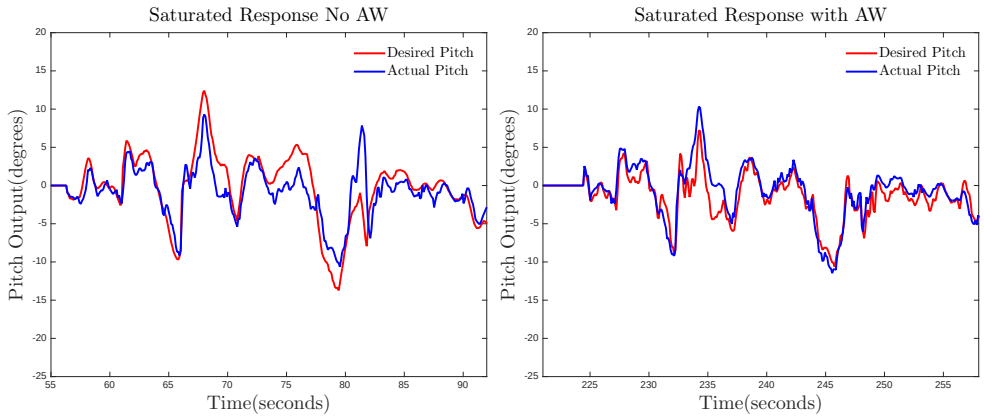

Fig. 19. **Full Flight Pitch response**: (a) [from left] **Saturated No AW**; (b) **Saturated, with AW (Section II-A)**

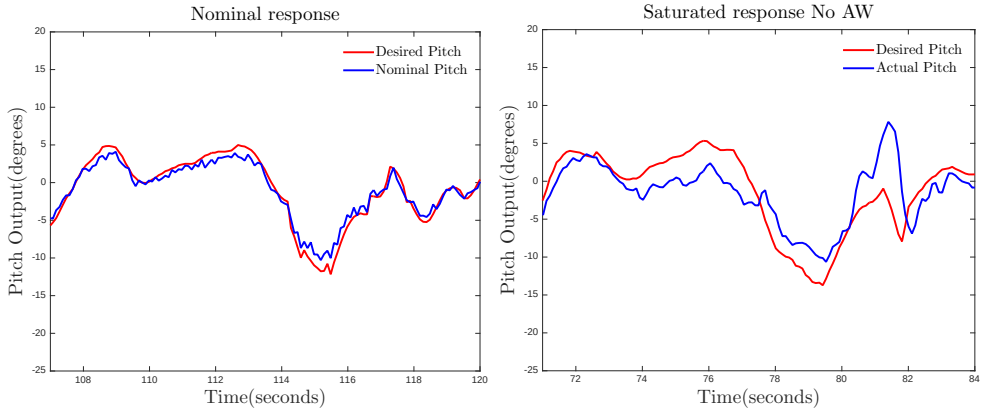

Fig. 20. **Focus on artificial limit flight section**: (a) [from left] **Nominal response** ; (b) **Saturated response no AW**

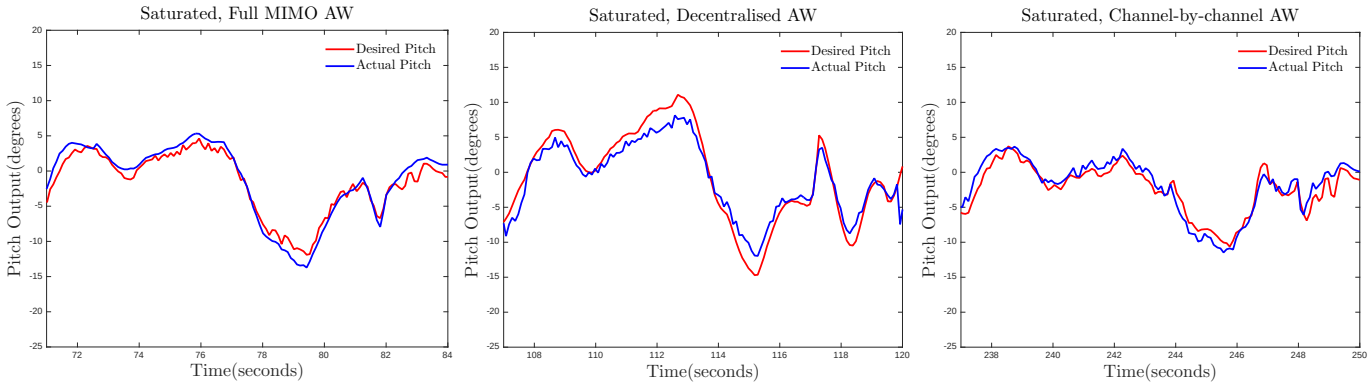

Fig. 21. Pitch angle response: (a) [from left] Saturation, **full MIMO AW (Section II-A)**; (b) Saturation, **decentralised AW** (Section III-A); (c) Saturation, **Channel-by-channel AW** (Section III-B)

the UAV is seen to jerk slightly along the pitch axis and becomes increasingly unstable with time.

Figures 21a, 21b and 21c show improved responses when the AW compensators are engaged using the full MIMO AW, decentralised AW and channel-by-channel AW compensators respectively. The pitch response overshoot seen in Figure 20b is largely reduced in all three cases of Figure 21 and its signals are now in phase with the desired/reference signal.

It is important to note that all flights are not exactly alike because with outdoor flights, gust, wind speed and other weather conditions are not constant and hence the differences between each of these plots.

VI. Conclusion

This paper has proposed two techniques for structured anti-windup compensator design for plants which exhibit a certain structure. The first (pseudo-decentralised) approach allows one to design an anti-windup compensator which, from the perspective of the virtual control signals, appears decentralised. The second (channel-by-channel) approach enables one to design separate single-loop anti-windup compensators and combine them in such a manner that they guarantee stability for the multivariable closed-loop system.

The paper has applied these decentralised approaches to saturation problems in a quadrotor UAV, both in simulation and in experiment. The results show that the pseudo-decentralised approaches to anti-windup design can all offer similar performance improvement, during saturation, as a standard multivariable anti-windup compensator. The crucial feature is that the channel-by-channel AW compensator can be designed and implemented for just one channel of the system thereby reducing the higher computational burden experienced when the other two AW compensator designed in this paper are implemented. Furthermore,in the channel-by-channel approach, each i'th single-loop compensators can be redesigned without affecting either the other compensators or the stability of the overall multivariable system.

References

[1] E. F. Mulder, M. V. Kothare, and M. Morari, "Multivariable anti-windup controller synthesis using linear matrix inequalities," *Automatica*, vol. 37, no. 9, pp. 1407–1416, 2001.

[2] G. Grimm, J. Hatfield, I. Postlethwaite, A. R. Teel, M. C. Turner, and L. Zaccarian, "Anti-windup for stable linear systems with input saturation: an lmi-based synthesis," *Automatic Control, IEEE Transactions on*, vol. 48, no. 9, pp. 1509–1525, 2003.

[3] J.-M. Biannic and S. Tarbouriech, "Optimisation and implementation of dynamic anti-windup compensators with multiple saturations in flight control systems," *Control Eng Pract*, vol. 17, no. 6, pp. 703–717, 2009.

[4] M. C. Turner, G. Herrmann, and I. Postlethwaite, "Incorporating robustness requirements into anti-windup design," *Automatic Control, IEEE Transactions on*, vol. 52, no. 10, pp. 1842–1855, 2007.

[5] A. Glattfelder and W. Schaufelberger, *Control systems with input and output constraints*. Springer, London, 2003.

[6] S. Tarbouriech, G. Garcia, J. M. Gomes da Silva Jr., and I. Queinnec, *Stability and Stabilization of Linear Systems with Saturating Actuators*. Springer, 2011.

[7] L. Zaccarian and A. Teel, *Modern Anti-windup Synthesis: Control Augmentation for Actuator Saturation*. New Jersey: Princeton University Press, 2011.

[8] S. Galeani, S. Tarbouriech, M. Turner, and L. Zaccarian, "A tutorial on modern anti-windup design," *European Journal of Control*, vol. 15, no. 3, pp. 418–440, 2009.

[9] A. Adegbege and W. Heath, "Internal model control design for input-constrained multivariable processes," *AIChE Journal*, vol. 57, pp. 3459–3472, 2011.

[10] A. A. Adegbege and W. P. Heath, "Directionality Compensation for Linear Multivariable Anti-windup Synthesis." *International Journal of Control*, no. just-accepted, pp. 1–24, 2015.

[11] C. Edwards and I. Postlethwaite, "Anti-windup and bumpless-transfer schemes," *Automatica*, vol. 34, no. 2, pp. 199–210, 1998.

[12] N. Ofodile, M. Turner, and O. Ubadike, "Channel-by-channel anti-windup design for a class of multivariable systems," in *American Control Conference Chicago, IL, USA*, 2015.

[13] S. Bouabdallah, P. Murrieri, and R. Siegwart, "Design and control of an indoor micro quadrotor," in *Robotics and Automation, 2004. Proceedings. ICRA'04. 2004 IEEE International Conference on*, vol. 5. IEEE, 2004, pp. 4393–4398.

[14] M. Cutler, N. K. Ure, B. Michini, and J. P. How, "Comparison of fixed and variable pitch actuators for agile quadrotors," in *AIAA Conf. on Guidance, Navigation and Control, Portland, OR*, 2011.

[15] M. Orsag, M. Poropat, and S. Bogdan, "Hybrid fly-by-wire quadrotor controller," *AUTOMATIKA: časopis za automatiku, mjerenje, elektroniku, računarstvo i komunikacije*, vol. 51, no. 1, pp. 19–32, 2010.

[16] J. Sofrony, M. C. Turner, and I. Postlethwaite, "Anti-windup synthesis using riccati equations," *International Journal of Control*, vol. 80, no. 1, pp. 112–128, 2007.

[17] P. F. Weston and I. Postlethwaite, "Linear conditioning for systems containing saturating actuators," *Automatica*, vol. 36, no. 9, pp. 1347–1354, 2000.

[18] M. C. Turner and I. Postlethwaite, "A new perspective on static and low order anti-windup synthesis," *International Journal of Control*, vol. 77, no. 1, pp. 27–44, 2004.

[19] C. F. V. Loan, "The ubiquitous kronecker product," *Journal of computational and applied mathematics*, vol. 123, no. 1, pp. 85–100, 2000.

[20] R. C. Leishman, J. C. Macdonald, R. W. Beard, and T. W. McLain, "Quadrotors and accelerometers: State estimation with an improved dynamic model," *Control Systems, IEEE*, vol. 34, no. 1, pp. 28–41, 2014.

[21] S. Bouabdallah and R. Siegwart, "Full control of a quadrotor," in *Intelligent robots and systems, 2007. IROS 2007. IEEE/RSJ international conference on*. IEEE, 2007, pp. 153–158.

[22] J. R. Azinheira and A. Moutinho, "Hover control of an UAV with backstepping design including input saturations," *Control Systems Technology, IEEE Transactions on*, vol. 16, no. 3, pp. 517–526, 2008.

[23] J. S. Jang, *Nonlinear control using discrete-time dynamic inversion under input saturation: theory and experiment on the Stanford dragonfly UAVs*. California USA: ProQuest Dissertations And Theses; Stanford University Press, 2004.

[24] W. Ren and R. W. Beard, "CLF-based tracking control for UAV kinematic models with saturation constraints," in *Decision and Control, 2003. Proceedings. 42nd IEEE Conference on*, vol. 4. IEEE, 2003, pp. 3924–3929.

[25] N. Kahveci, P. Ioannou, and M. Mirmirani, "Adaptive LQ Control With Anti-Windup Augmentation to Optimize UAV Performance in Autonomous Soaring Applications," *IEEE Transactions on Control Systems Technology*, vol. 16, no. 4, pp. 691–707, 2008.

[26] R. W. Beard, "Quadrotor dynamics and control," Brigham Young University, Utah USA, Tech. Rep., February 2008.

[27] UnmannedTech.co.uk, "2014 3DR Quad Kit." [Online]. Available: http://www.unmannedtechshop.co.uk/arducopter-3dr-quad-diy-frame, Accessed on: Nov. 11, 2014

[28] H. K. Khalil, "Nonlinear systems, 3rd edition," *New Jewsey, Prentice Hall*, vol. 9, 2002.

Appendix A
Proof of Theorem 3

As mentioned earlier, the stability and performance of the system in Figure 7 reduces to guaranteeing the stability and performance of the nonlinear operator $\mathcal{T}_p$. In the case of the decentralised anti-windup compensator, a state-space realisation of $\mathcal{T}_p$ is given by

$$\dot{x}_D = (A_D + B_D F_D)x_D + B_D\tilde{\chi}(v) \tag{50}$$

$$v_d = F_D x_D \tag{51}$$

$$y_d = (C_D + D_D F_D)x_D + D_D\tilde{\chi}(v) \tag{52}$$

where

$$\tilde{\chi}(v) = XDz[X^{-1}(v_{lin} - v_d)]. \tag{53}$$

To guarantee stability and ensure that $\|\mathcal{T}_p\|_{i,2} < \gamma$, it is sufficient for the following inequality to hold for some Lyapunov function $V(x)$ and some scalar $\gamma > 0$,

$$\dot{V}(x) - \gamma\|v_{lin}\|^2 + \frac{1}{\gamma}\|y_d\|^2 < 0. \tag{54}$$

Recall that as the deadzone inequality belongs to the Sector $[0,\ I]$, for some diagonal matrix $W > 0$ [28], the following inequality

$$\Omega(v) = \mathrm{Dz}(X^{-1}v)'W\left(v - \mathrm{Dz}(X^{-1}v)\right) \geq 0 \tag{55}$$

holds. The Lyapunov function is chosen as $V(x_D) = x_D' P_D x_D$ where P_D is a positive definite block diagonal matrix, with elements of dimensions consistent with (A_D, B_D, C_D). By appending the sector inequality (55) to (54), we require

$$\dot{V}(x_D) - \gamma\|v_{lin}\|^2 + \frac{1}{\gamma}\|y_d\|^2 + \Omega(v) < 0. \tag{56}$$

Using the realisation (52) and noting $v = v_{lin} - v_d$, similar to [18] we obtain the linear matrix inequality in (24). This LMI is obtained after evaluating the inequality (56) using standard Schur complements and the congruence transformation $\mathrm{diag}(P_D^{-1}, W^{-1}, I, I) = \mathrm{diag}(Q_D, U_D, I, I)$.

Appendix B
Proof of Lemma 1

Since $\tilde{\chi}(u) := X\mathrm{Dz}(X^{-1}u)$, the left hand side of the inequality (35) can then be written as

$$\begin{aligned}\text{l.h.s.}(35) &= \mathrm{Dz}(X^{-1}u)'X'W[u - X\mathrm{Dz}(X^{-1}u)] \\ &= \mathrm{Dz}(X^{-1}u)'X'WX[X^{-1}u - \mathrm{Dz}(X^{-1}u)]. \end{aligned}\tag{57}$$

Substituting $u_x = X^{-1}u$ and $V = X'WX$ in the equation above results in,

$$\tilde{\chi}(u)'W\left(u - \tilde{\chi}(u)\right) = \mathrm{Dz}(u_x)V[u_x - \mathrm{Dz}(u_x)]. \tag{58}$$

It then follows that for any u_x and any diagonal $V > 0$, the inequality,

$$\mathrm{Dz}(u_x)'V[u_x - \mathrm{Dz}(u_x)] > 0 \quad \forall u_x \in \mathbb{R}^m \tag{59}$$

holds by virtue of the deadzone's sector property. Hence, in order for the inequality (35) to hold, it is sufficient for there to exist diagonal matrices $W > 0$ and $V > 0$ satisfying equation (34).

Appendix C
Proof of Theorem 4

The state space realization of each i^{th} loop of $\Theta(s)$ in (32) is

$$\dot{x}_i = (A_i + B_iF_i)x_i + B_i\tilde{\chi}_i(u) \tag{60}$$
$$u_i = F_ix_i \tag{61}$$
$$y_i = (C_i + D_iF_i)x_i + D_i\tilde{\chi}(u). \tag{62}$$

By choosing the Lyapunov function $V(x) = x'P_Dx = \sum_{i=1}^m x_i'P_ix_i$, $\dot{V}(x)$ becomes

$$\begin{aligned}\dot{V}(x) =& x'\left((A_D + B_DF_D)'P_D + P_D(A_D + B_DF_D)\right)x \\ &+ 2x'P_DB_D\tilde{\chi}(u). \end{aligned}\tag{63}$$

Using Lemma 1, it follows that there exists a diagonal $W > 0$ such that

$$\tilde{\chi}(u)'W\left(u - \tilde{\chi}(u)\right) \geq 0, \qquad \forall u \in \mathbb{R}^m. \tag{64}$$

Therefore, a sufficient condition for inequality (63) to hold is for the inequality below to hold:

$$\dot{V}(x) \leq \begin{bmatrix} x \\ \tilde{\chi}(u)\end{bmatrix}'\mathrm{He}\left\{\begin{bmatrix} P_D(A_D + B_DF_D) & P_DB_D \\ -WF_D & -W\end{bmatrix}\right\}\begin{bmatrix} x \\ \tilde{\chi}(u)\end{bmatrix}. \tag{65}$$

Due to the diagonal nature of all the matrices, this inequality can be broken down into

$$\dot{V}(x) \leq \sum_{i=1}^m \begin{bmatrix} x_i \\ \tilde{\chi}_i(u)\end{bmatrix}'\mathrm{He}\left\{\begin{bmatrix} P_i(A_i + B_iF_i) & P_iB_i \\ -W_iF_i & -W_i\end{bmatrix}\right\}\begin{bmatrix} x_i \\ \tilde{\chi}_i(u)\end{bmatrix}. \tag{66}$$

After applying standard Schur complements and the congruence transformation $\mathrm{diag}(P_i^{-1}, W_i^{-1}) = \mathrm{diag}(Q_i, U_i)$, we obtain the LMI (8).